Geologia Croatica
Journal of the Croatian Geological Survey and the Croatian Geological Society
2025 | 78/1 | 45–60 | 7 Figs. | 2 Tabs. | 2 Suppls. | www.geologia-croatica.hr

Microstructures of feldspar crystals from Pakra Creek valley granite (Papuk Mt., Croatia)

Marija Horvat[1,*], Viktória Kovács Kis[2] and Jasmina Martinčević Lazar[1]

[1] Croatian Geological Survey, Department of Geology, Sachsova 2, 10000 Zagreb, Croatia; (jmartincevic@hgi-cgs.hr; *corresponding author: mhorvat@hgi-cgs.hr)
[2] HUN-REN Centre for Energy Research, Konkoly-Thege Miklós út 29-33, H-1121, Budapest, Hungary; (kis.viktoria@ek.hun-ren.hu)

doi: 10.4154/gc.2025.06

Article history:
Manuscript received: November 15, 2024
Revised manuscript accepted: January 21, 2025
Available online: February 27, 2025

Keywords: microstructure, feldspar, granite, Pakra Creek valley, Papuk Mt., Croatia

Abstract

Optical polarizing microscopy, X-ray powder diffraction and transmission electron microscopy with energy-dispersive spectroscopy have been used to study microstructures in feldspars from two structurally and texturally different granite types from Pakra Creek valley (Papuk Mt., Croatia). The porphyritic texture granite contains pink potassium feldspar megacrysts with cross-hatched extinction and tweed pattern, which proved to be intermediate microcline to orthoclase. These crystals have Or > 90% and An=0 composition, and coexist with low albite Or(1.2)Ab(98.8)An(0). The feldspars from the granite with homogenous fine-grained microstructure are white in colour and proved to be mixture of lamellar and zoned plagioclase and intermediate microcline. The plagioclase has a Na:Ca ratio close to 3:1 and minor K content (72.2%<Ab<76.5%, 23%<An<26.8%, Or<1.4%). Pure albite (Ab=97-99%) and anorthite (An=99%) grains were also detected. The higher content of plagioclase in the granite with homogenous fine-grained microstructure indicates a higher crystallization temperature compared to the porphyritic type. The microstructure of the feldspar crystals suggests a parent melt close to the eutectic composition for the studied granites.

1. INTRODUCTION

In the literature there are many suggestions how to make distinction between different potassium feldspar "mineral species", but the International Mineralogical Association (IMA) recommends three terms: "sanidine", "orthoclase" and "microcline" (BARTH, 1934). "Microcline" (K>>Na)$AlSi_3O_8$ is the low-temperature phase. The crystal structure is triclinic $C\bar{1}$ with four crystallographic tetrahedral (T) sites with an ordered Si, Al distribution. Orthoclase has monoclinic C2/m symmetry, according to the disordered distribution of Al and Si between the four T sites. Mineral species and mineral varieties can be characterized by various techniques. Under equilibrium conditions, LAVES & GOLDSMITH (1961) distinguishes the following K-feldspars: low microcline, intermediate microcline and high microcline. Based on X-ray powder diffraction (XRPD), RIBBE (1983) classifies them as low microcline, intermediate microcline and orthoclase. Using selected area (electron) diffraction (SAED), BAMBAUER et al. (1989) identified K-feldspars based on their scattering characteristics in [001] zone projection, as a) regular microcline twinning, A (Albite law) and P (Pericline law) twins spot splitting; b) irregular twinning microcline (A and P twins spot splitting and diffuse streaks; and c) tweed (domains) orthoclase (A and P twins diffuse streaks). STEWART & RIBBE (1983) distinguished optical microcline (δδ0δ) and optical orthoclase (δ=0δ) by polarized light optical microscopy (PLOM) according to the extinction angle δ in (001) sections. According to SÁNCHEZ-MUÑOZ et al. (2012) microcline is characterized by a low crystallization temperature, triclinic symmetry and ordered Si, Al distribution, while orthoclase is metastable having triclinic-like symmetry, with partially ordered Si, Al distribution, which leads to the formation of modulations in structural strain. The same authors highlight the significance of a high content of chemical hinderers in orthoclase, which act as a barrier to structural ordering. The fine grainsize of granite WEBBER et al. (1999) connected to a drop in pressure and rapid cooling at high crustal levels (ROCKHOLD et al., 1987). WILLAIME et al. (1976) described a complete list of potassium feldspar microstructures depending on the melt composition and cooling rate.

Potassium feldspar megacrysts are very common in granitic rocks, being either triclinic microcline or monoclinic orthoclase. KERRICK (1969) firstly expressed an opinion that potassium feldspar megacrysts crystallize from the melt in the early phase of magma solidification compared to the groundmass microcline. VERNON (1986), BATEMAN (1992) and COX et al. (1996) later confirmed this theory. VERNON (1986) and COX et al. (1996) linked Ba-oscillatory zoning in potassium feldspar megacrysts to their igneous crystallization. DICKSON & SABINE (1967) and JOHNSON et al. (2006a, b) attributed their crystallization to a late water-rich fluid phase under subsolidus conditions as porphyroblasts and replacement of other mineral grains. COLLINS & COLLINS (2002, and references therein) suggested microcline replacements of plagioclase and formation of myrmekite due to the influence of potassium bearing fluids. COLEMAN et al. (2005) and GLAZNER et al. (2004) reported that a porphyroblastic origin is necessary in the post solidification phase, and that the igneous origin of the megacrysts is compatible with the host pluton. GLAZNER et al. (2004) also introduced the term "big tank"

crystallizing reservoir of magma and gave examples that the potassium feldspars mostly grow after the magma crosses the rheological lock-up threshold of ≈ 50% crystals (GLAZNER & JOHNSON, 2013). Further, the same authors stated that the high potassium composition of megacrysts and their large size possibly required growth temperatures below the nominal solidus temperatures of ≈ 650 °C and exsolution of Ab (albite) component down to temperatures of ≈ 400 °C. BROWN & PARSONS (1989) and PARSONS et al. (2015), discusses exsolution and twin microstructures in alkali feldspars in relation to their thermal history including behaviour during diagenesis and weathering. They also emphasize that phase equilibria and thermodynamics of reactions should be considered as appropriate, i.e. taking into account the effect of interfaces and particle size and stability in oxide-bearing systems (NAVROTSKY et al., 2008; NAVROTSKY, 2011; KONTONIKAS-CHAROS et al., 2018). The first report about alkali feldspar megacrysts from Pakra Creek (Papuk Mt., Croatia) was given in KUČAN & KRMPOTIĆ (1911). They described them in a gneiss host as "microcline-microperthites". POLJAK (1952) mentioned up to 5 cm feldspar crystals in the Pakra Creek valley granites. The "large pink microcline" crystals from pegmatitic pockets (Sloboština Creek) and granitic veins (Pakra Creek) were later studied by TAJDER (1957). The megacrysts in adamellite and granodiorite of West Papuk Mt. as porphyritic and vein filling, diffuse, metasomatic K-feldspar megacrysts were described by VRAGOVIĆ (1965).

Two types of megacrysts, vein filling (Pakra Creek, Papuk Mt.) and pocket forming (Sloboština Creek, Papuk Mt.), were studied by KOVÁCS KIS et al. (2004), and proved to be low microcline in association with low albite and quartz. The alkali feldspar megacryst from Pakra Creek was characterised by the absence of twinning, while the megacryst from Sloboština Creek showed a tweed-like texture (KOVÁCS KIS et al., 2004). The deduced crystallization temperatures were below 460 °C, and near to but above 460 °C, respectively. These low microcline megacrysts are characterised by a continuously modulated lattice on the submicroscopic scale.

The main aim of this paper is determining the type of feldspars and their microstructure in two different granite types (sample 2PPG-4, the porphyritic, and PPG-24 the homogeneous type), both from Pakra Creek valley, Papuk Mt. (Fig. 1). These two different types of feldspar host rocks were chosen for this study, which are representative of granites in the Pakra Creek valley and associated with pegmatite occurrence described in KOVÁCS KIS et al. (2004). These results will be useful for the further study of a series of granites and associated migmatite and metamorphic samples, and will provide details of the geological history of the area.

2. METHODS

The chemical and structural inhomogeneity of the feldspar grains were measured using a polarizing microscope (PM), X-ray powder diffractometer (XRPD) and a transmission electron microscope (TEM).

The modal composition was determined using a polarizing microscope Zeiss Axio Lab A1 equipped with an ocular net and Zeiss Axiocam 105 digital camera with software ZEN at

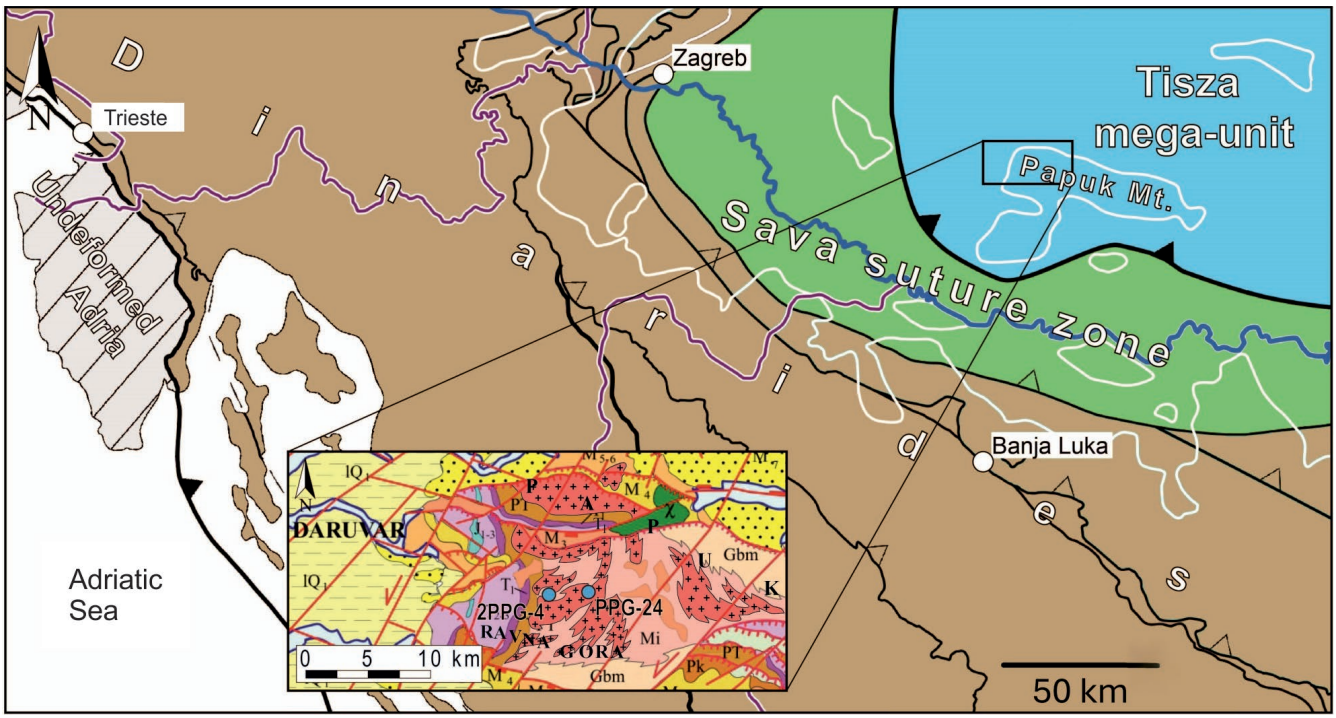

Figure 1. The sampling localities (blue circles) in the Pakra Creek valley (Papuk Mt.) on the compiled geological map of Slavonian Mts. (JAMIČIĆ, 2001) and their position within the Tisza mega-unit on the tectonic map of SCHMID et al. (2020). Lithology legend for the geological map: Pk – chlorite-sericite schist, metagabbro, marble, amphibolite, amphibole schist, phlaseride granitoid, garnet-staurolite gneiss; Mi – migmatite; Gbm – garnet-biotite-muscovite gneiss; + granitoids (symbol from HORVAT, 2004); D,C – graphitic schist, conglomerate, sandstone; PT – quartz sandstone, conglomerate; T_1 – sandstone, siltstone, shale; T_{2-3} – dolomite, dolomitic limestone; J_{1-3} – limestone; M_2 – conglomerate, sand, gravel; M_3 – conglomerate, sand, clay and marl; M_4 – conglomerate, limestone, marl; M_{5-6} – marl and limestone; M_7 – sand, marl and clay; χ – albite rhyolite, andesite, basalt; Pl,Q – gravel and sands; lQ_1 – loess; dprQ2 – deluvial-proluvial deposits; aQ_2 – alluvium of creeks.

the Department of Geology of Croatian Geological Survey. The value of standard deviations of repeated measurements was below 3%.

The X-ray powder diffraction (XRPD) measurements of crystals extracted from the granite rock (grains *a* and *b*, sample 2PPG-4) and non-magnetic, low density fraction of whole rock PPG-24 sample, were performed on a SIEMENS 0500 powder diffractometer (Cu radiation, 40kV, 20 mA, analogous registration at 0.5° 2θ/min goniometer speed), at the Department of Mineralogy of Eötvös Loránd University. For the d-value measurements, the reflections of accompanying quartz (PDF 00-033-1161) were used as an inner standard. The X-ray powder diffraction (XRPD) measurements were performed additionally for megacrysts (grain *c*) and a whole rock sample 2PPG-4 with a PANalytical X' Pert PRO diffractometer at the Department of Geology, Croatian Geological Survey (Cu-tube, graphite monochromator and Pixel detector; experimental conditions: 45 kV, 40 mA, PW 3018/00 PIXcel detector, primary beam divergence 1°, and continuous scan step 0.02° 2θ/s). The program X'Pert HighScore Plus (PANalytical, 2016) was used, which contains powder diffraction database PDF 4/ Minerals (International Centre for Diffraction data, 2024).

Powder samples for TEM were prepared from large sized crystals which appear to be homogeneous both with the naked eye and under an optical microscope. Special attention was paid to select pieces that could be considered representative of the large, macroscopic crystals. However, the presence of a minor, non-representative sample volume in the TEM specimen cannot be ruled out. Therefore, for SAED and (HR)TEM analysis, only such grains were used, which proved to be the major component based on the comparison of TEM-EDS and XRD data.

The samples for TEM observations were obtained by grinding the sample under ethanol and mounting a drop from the suspension onto a Cu-grid covered by amorphous carbon supporting film.

TEM study was done at the HUN-REN Centre for Energy Research, Budapest, Hungary, using a Themis (ThermoFisher) TEM, operated at 200 kV and equipped with Cs (spherical aberration) correction in the imaging system (spatial resolution in HRTEM mode 0.8 Å). The microscope is equipped with a

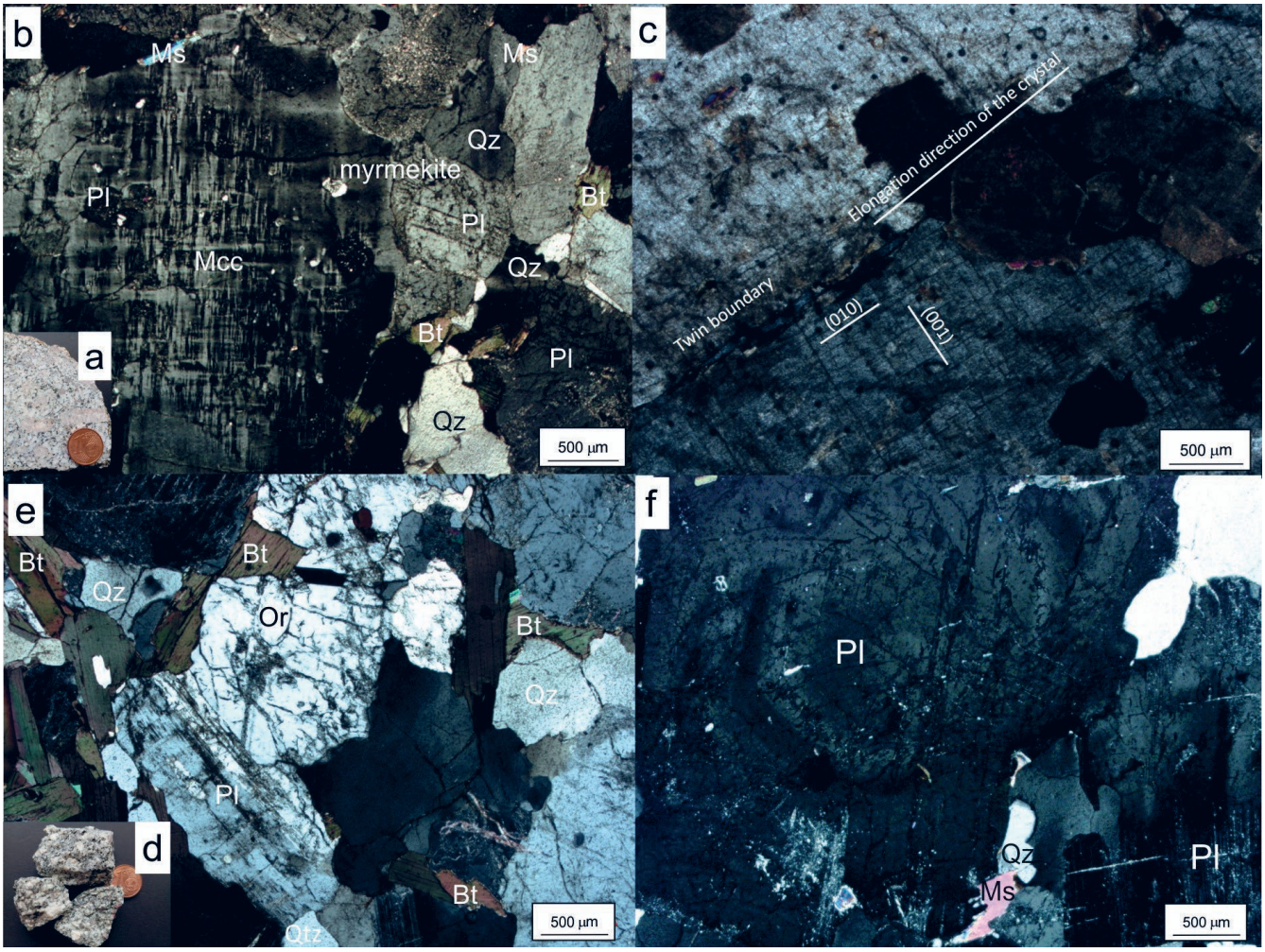

Figure 2. a) The sample 2PPG-4 image; **b, c)** Photomicrographs of porphyritic structure sample 2PPG-4, XPL – cross-polarized light; **b)** The microcline, plagioclase, quartz, biotite, muscovite presence and myrmekite occurrence; **c)** alkali feldspar cross-hatched extinction pattern; perfect cleavage along {001}, good cleavage along {010} are observed. Right angle cleavage is characteristic; both twin systems extinct simultaneously; **d)** The sample PPG-24 image; **e, f)** Photomicrographs of the homogeneous structured PPG-24 sample, XPL – cross-polarized light; **e)** The orthoclase, plagioclase, quartz, biotite and muscovite presence; **f)** Plagioclase exhibits compositional zonation as well. Abbreviations are according WARR (2021): Bt – biotite, Mcc – microcline, Ms – muscovite, Or – orthoclase, Pl – plagioclase and Qz – quartz. Diameter of the coin is 1.6 cm.

Schottky field emission gun (FEG) having an energy spread of 0.7 eV. SAED patterns were taken from an area of 600 nm diameter and recorded using a 4kx4k Ceta camera and Velox software (Thermo Fisher). Offline analysis of SAED patterns and Fast Fourier Transform (FFT) analysis of high resolution (HR)TEM images was undertaken with Velox software (Thermo Fisher) and CRISP software (Calidris, Sollentuna, Sweden) (HOVMÖLLER, 1992). Calculation of SAED patterns was done using the SingleCrystal 4.1.7 software (CrystalMaker Software Limited, Begbroke, UK).

3. RESULTS

The sample 2PPG-4 contains pink feldspar megacrysts measuring up to 2x1 cm size, and this granite has a porphyritic texture (Fig. 2a). Besides the pink megacrysts, a white mineral, hypidiomorphic to allotriomorphic in shape is also considered to be a feldspar. The sample contains biotite flakes and grey quartz grains. Biotite is a few mm and quartz is up to 1 cm in size (Fig. 2a). The second granite sample PPG-24 has a homogeneous structure and is composed of grains with a uniform grain size distribution measuring from 1 to 5 mm (Fig. 2d). The sample contains grey quartz, black biotite and white minerals, assumed to be feldspars of different cross-section sizes (Fig. 2d).

The porphyritic granite with pink megacrysts (sample 2PPG-4) has the following modal composition: microcline 32%, orthoclase 8%, plagioclase 43%, quartz 8%, biotite 5%, muscovite below 1% and chlorite below 1%. Polarized light microscope observations confirm two generations of potassium feldspar, the early phase being a feldspar within the potassium feldspar megacryst with cross-hatched extinction pattern (Fig. 2b). This extinction pattern is characteristic for microcline twinning (Fig. 2c), which is regarded as a result of orthoclase-to-microcline solid-state transformation (LAVES, 1950; McLAREN, 1984).

In the sample PPG-24, orthoclase grains can be distinguished besides plagioclase according to polarized light microscopy (Fig. 2e). This sample has the following modal composition: plagioclase 63%, orthoclase 16%, quartz 9%, biotite 10% and chlorite under 2%. Besides lamellar plagioclase grains (Fig. 2e), zoned plagioclase also occurs (Fig. 2f).

Three pink megacrysts and whole rock of 2PPG-4 sample, and white feldspar from non-magnetic, low-density fraction of PPG-24 sample were analysed with XRPD. The reference diffraction data were: quartz (MORRIS et al., 1981), intermediate microcline (BORG & SMITH, 1969), orthoclase (BORG & SMITH, 1969), albite, calcian (BORG & SMITH, 1968), mica (GRIM et al., 1937) in BROWN (1961), albite (SMITH, 1956), orthoclase (PRINCE et al., 1973), microcline (ALLAN et al., 1997) and quartz (PAKHOMOV et al., 1993). For the 2PPG-4 sample grains XRPD patterns showed orthoclase and microcline, minor quartz, albite and mica (Table 1, Fig. 3). The diffraction pattern of the whole rock 2PPG-4 sample yielded microcline, minor quartz, albite and mica (Table 1). The triclinic symmetry of microcline manifests in the Δ131Δ reflection splitting into (131) and ($1\bar{3}1$) at the following d-values: 3.015(3.025) Å and 2.980(2.996) Å (Fig. 3, Table 1). The value of triclinicity ($\Delta = d_{(131)} - d_{(1\text{-}31)} * 12.5$) is 0.44 (grain *a*) and 0.36 (grain c) calculated according to GOLDSMITH & LAVES (1954). Low albite peaks appear at the following

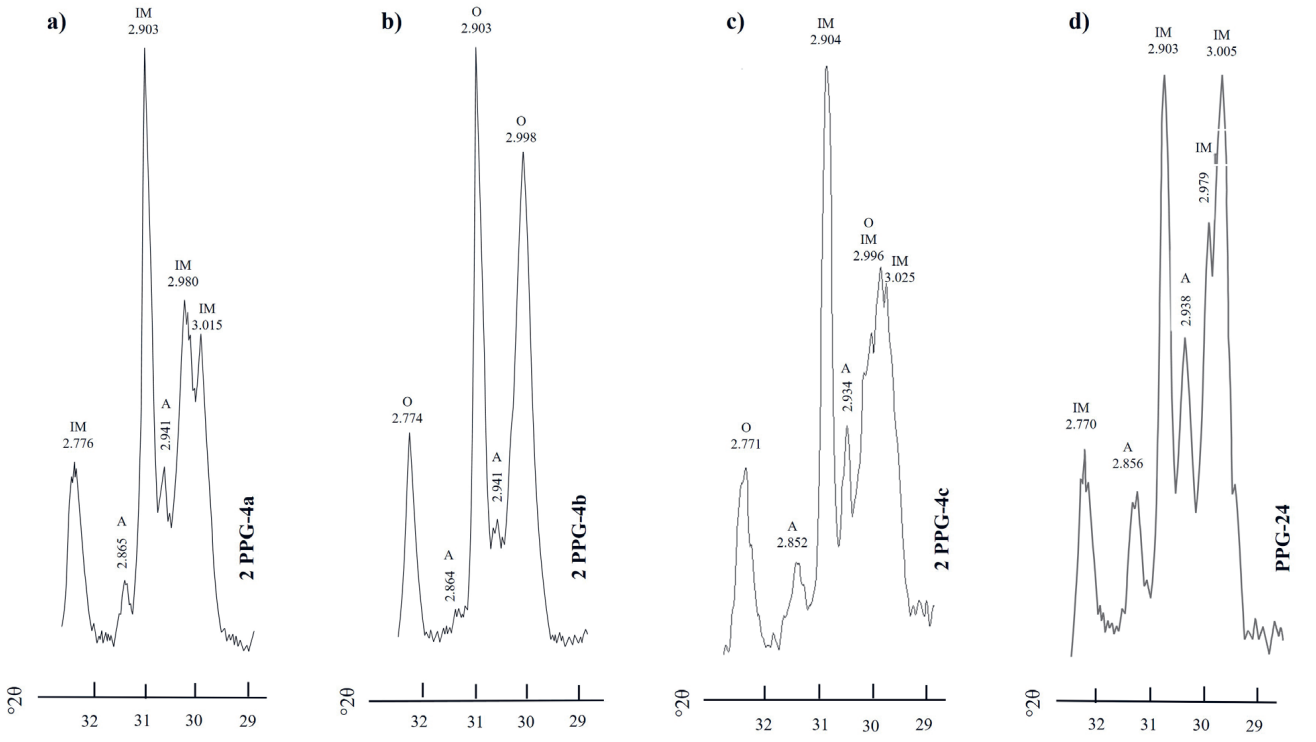

Figure 3. XRPD analysis magnified detail of {131} diffraction region: **a)** pink megacryst extracted from the granite sample 2PPG-4 (grain a, this study); **b)** pink megacryst extracted from the granite sample 2PPG-4 (grain b, this study); **c)** pink megacryst extracted from the granite sample 2PPG-4 (grain c, this study); **d)** non-magnetic, low-density fractions of whole rock PPG-24 sample (taken from HORVAT et al., 2011). The related data set is in Table 1) IM – intermediate microcline; O – orthoclase; A – albite; *d* values in Ångströms.

Table 1. XRPD data sets of three pink megacrysts and whole-rock of the 2PPG-4 sample and non-magnetic, low density fractions of whole rock PPG-24 sample. The reference diffraction data for 2PPG-4 grains *a* and *b*, and PPG-24 sample: quartz (MORRIS et al., 1981), intermediate microcline (BORG & SMITH, 1969), orthoclase (BORG & SMITH, 1969), albite, calcian (BORG & SMITH, 1968), mica (GRIM et al., 1937) in BROWN (1961); grain *c* and whole rock of 2PPG-4 sample: albite (SMITH, 1956), albite, calcian (BORG & SMITH, 1968), orthoclase (PRINCE et al., 1973), microcline (ALLAN et al., 1997), quartz (PAKHOMOV et al., 1993). Legend: d_{ob} – observed reflection, I_{lit} – reflection intensity (literature data), s – strong intensity.

d_{ob} (Å) 2PPG-4a	d_{ob} (Å) 2PPG-4b	d_{ob} (Å) 2PPG-4c	d_{ob} (Å) 2PPG-4	d_{ob} (Å) PPG-24	$I_{relative}$ 2PPG-4a	$I_{relative}$ 2PPG-4b	$I_{relative}$ 2PPG-4c	$I_{relative}$ 2PPG-4	$I_{relative}$ PPG-24	mineral	d_{lit} (Å)	hkl	I_{lit}
10.03	10.03	10.07	10.09	10.01	0.6	1.1	0.8	4.0	0.8	mica	9.99	002	s
6.510	6.510	6.489	6.498	6.487	5.5	5.9	1.8	0.6	4.3	intermediate microcline/orthoclase/ microcline	6.483/6.498/ 6.482	001/020	6/7/7.9
-	-	6.396	6.390	6.412	-	-	0.5	1.2	0.8	albite/albite-Ca	6.390	001	20
5.941	5.910	5.892	5.877	5.906	1.2	1.6	0.5	0.6	0.8	intermediate microcline/orthoclase/ microcline/albite/albite-Ca	5.893/5.861	$\bar{1}\bar{1}1/\bar{1}11$	5/7
4.613	4.603	4.592	4.603	4.594	1.2	1.3	0.2	0.3	0.7	intermediate microcline/orthoclase/ microcline	4.587/4.583	$0\bar{2}1/021$	3/2
4.234	4.228	4.228	4.233	4.230	8.7	12.7	2.4	8.3	7	intermediate microcline/orthoclase/ microcline	4.257/4.217	$100/\bar{2}01$	22/61
4.045	4.045	4.037	4.041	4.042	2.7	3.1	1.1	8.7	5	albite/albite-Ca	4.030	$\bar{2}01$	16/52
3.970	3.956	3.956	3.955	3.951	5.5	7.7	1.1	1.6	3.7	intermediate microcline/microcline	3.961	111	11/10
3.870	3.863	3.860	3.874	3.866	2.5	2.6	0.6	1.7	2	albite/albite-Ca	3.857	$1\bar{1}1$	8
3.792	3.785	3.778	3.771	3.787	8.6	15	2.3	9.5	9.7	intermediate microcline/albite/ orthoclase/albite-Ca	3.792/3.780/ 3.775	130/111/130	36/25/75
3.765	3.679	3.718	3.718	-	7.7	1.3	0.7	5.8	-	intermediate microcline/albite/ albite-Ca	3.746/3.657	$\bar{1}30/200$	37/18
3.677	3.642	3.666	3.664	3.665	2.9	1.3	0.9	5.1	3.9	albite/albite-Ca	3.663	$\bar{1}\bar{3}1$	16
3.618	3.639	3.597	3.598	-	1.5	0.7	0.7	0.7	-	intermediate microcline/orthoclase/ microcline	3.629	$\bar{1}\bar{3}1$	12
-	3.564	3.541	3.538	3.575	-	0.7	0.4	0.9	0.6	orthoclase/microcline	3.563/3.536	$\bar{2}21/\bar{2}\bar{2}1$	9
3.479	3.483	3.477	3.475	3.469	21	26	4.5	6.3	21.7	intermediate microcline/orthoclase/ microcline	3.477	$\bar{1}\bar{1}2$	46
3.344	3.341	3.345	3.347	3.340	16	19	16	100	32	quartz/intermediate microcline/ microcline	3.342/3.335	101/220	53
3.296	3.326	3.293	3.295	3.302	17	16	5	7.3	14	intermediate microcline/orthoclase/ microcline	3.293/3.335	$\bar{2}20/220$	50/53
3.244	3.305/ 3.244	3.243	3.243	3.252	100/19	24/100	100	25.6	100	intermediate microcline/orthoclase/ microcline	3.310/3.242	220/002	100/97
3.195	3.198	3.194	3.208	3.197	100	26	13.4	18.0	30	albite/albite-Ca	3.196	002	100

d_{ob} (Å) 2PPG-4a	d_{ob} (Å) 2PPG-4b	d_{ob} (Å) 2PPG-4c	d_{ob} (Å) 2PPG-4	d_{ob} (Å) PPG-24	$I_{relative}$ 2PPG-4a	$I_{relative}$ 2PPG-4b	$I_{relative}$ 2PPG-4c	$I_{relative}$ 2PPG-4	$I_{relative}$ PPG-24	mineral	d_{lit} (Å)	hkl	I_{lit}
3.015	-	3.025	-	3.005	6.5	-	0.4	-	7.1	intermediate microcline	3.005	131	26
2.980	2.998	2.996	2.997	2.979	7.1	12	2	5.3	5.2	intermediate microcline/orthoclase/ albite-Ca	2.979/2.991	$1\bar{3}1$/131	29/54
2.941	2.941	2.934	2.938	2.938	3.5	3	1	5.8	3.8	albite/albite-Ca	2.946	$0\bar{2}2$	5
2.903	2.903	2.904	2.903	2.903	12	15	3	3.7	7	intermediate microcline/microcline	2.900	041	27
2.865	2.864	2.852	2.849	2.856	1.4	0.6	0.4	2.3	1.8	albite/albite-Ca	2.866	131	8
2.776	2.774	2.771	2.771	2.770	3.9	5.4	1	1.6	2.6	intermediate microcline/microcline	2.774	$\bar{1}\bar{3}2$	11
2.599	2.589	2.597	2.61	2.593	3.9	4.4	1	1.6	2.5	intermediate microcline/orthoclase/ microcline	2.589 2.593	$\bar{2}\bar{4}1$/221	19
2.563	2.562	2.557	2.559	2.556	7.5	7.8	1.8	5.0	2.5	intermediate microcline/orthoclase/ microcline	2.560	112	21/10
2.533	2.529	2.521	2.520	2.535	2	2.5	0.83	2.2	3.4	intermediate microcline/albite-Ca	2.528	310	5
2.463	-	2.457	2.458	2.461	0.8	-	0.96	6.8	1.4	quartz	2.457	110	8
2.425	2.423	2.421	2.434	2.424	1.5	1.9	0.35	1.5	1.4	intermediate microcline/albite-Ca	2.420	$\bar{1}51$	5
2.413	2.408	-	2.404	2.408	1.5	1.9	-	0.8	1.3	albite-Ca	2.403	$\bar{3}31$	7
2.335	2.333	2.330	2.330	2.332	2.8	3	0.89	1.5	1.8	intermediate microcline/orthoclase/ albite-Ca/microcline	2.330	$\bar{1}\bar{1}3$	6
2.285	2.284	2.282	2.28	2.284	0.8	0.9	1.28	8.2	1.1	quartz	2.282	102	8
2.196	-	2.190	2.210	-	0.7	-	0.15	0.5	-	albite-Ca/intermediate microcline	2.189	$1\bar{5}1$	3
2.166	2.165	2.162	2.164	2.163	10.8	9	5.23	3.8	6	intermediate microcline/orthoclase/ microcline	2.160	060	17
2.133	2.127	2.137	2.136	2.136	1.8	2.7	0.77	2.5	1.5	albite-Ca	2.137	241	5
2.119	2.122	2.129	2.129	2.117	1.8	2.7	1.44	9.5	2	quartz/albite/intermediate microcline/ orthoclase	2.127/2.114	200/$2\bar{4}1$	6/9
2.080	2.075	2.074	2.107	2.074	1.2	1.7	0.78	3.0	1	intermediate microcline/ orthoclase/ albite-Ca	2.074	$\bar{1}33$	4
2.061	2.057	2.052	2.049	2.053	1.2	2	0.46	0.5	1	intermediate microcline/ orthoclase/ microcline	2.050	061	4

Table 2. List of triclinicity values (α=12.5*αd(131)-d(1$\bar{3}$1α) calculated according to GOLDSMITH & LAVES (1954), for potassium feldspars from non-magnetic, low density fractions of whole rock (homogeneous rock type) and megacrysts (porphyritic rock type) of granites from Pakra Creek valley (Papuk Mt., Croatia).

	Sample name	Rock type	Δ calculated triclinicity
1	2PPG-4 (a)	porphyritic	0.44
2	2PPG-4 (b)*	porphyritic	0
3	2PPG-4 (c)	porphyritic	0.36
4	PPG-24*	homogeneous	0.32
5	2PPG-3*	porphyritic	0
6	2PPG-5*	porphyritic	0.29
7	2PPG-6 (a)*	porphyritic	0
8	2PPG-6 (b)*	porphyritic	0
9	PPG-19*	homogeneous	0
10	PPG-18*	homogeneous	0.87
11	PPG-20*	homogeneous	0.70
12	PPG-23*	homogeneous	0.56

*triclinicity values from HORVAT et al. (2011)

d-values: 4.04 Å, 3.87(3.86) Å, 3.64(3.68) Å, 3.19 Å, 2.93(2.94) Å and 2.85(2.86) Å (Table 1). One pink grain was determined as orthoclase (grain *b*). These results, together with the triclinicity values obtained and calculated in the previous study (HORVAT et al., 2011) indicate lower triclinicity values for potassium feldspars from porphyritic and high(er) triclinicity values for the potassium feldspars from homogeneous granite types (Table 2).

According to XRPD analysis, the white feldspar from PPG-24 sample proved to be mixture of intermediate microcline and plagioclase with a composition of Ab=71%, An=29% (BORG & SMITH, 1968) albite, Ca-bearing, ordered (Table 1). Besides feldspar phases, minor mica and quartz were detected. Triclinicity of the microcline component is 0.32 (Table 2).

By using TEM methods, crystal chemical details averaged out by XRD can be studied, which potentially provides a more precise crystallization history of these feldspar crystals. During the TEM EDS study of the 2PPG-4 sample mostly crystals with Or > 90% and An=0 composition were measured (for detailed measurement data see Suppl. 1), besides that only one grain with albite composition Or(1.2)Ab(98.8)An(0), and low albite structure was found. Figure 4 shows the characteristic microstructure of crystals with high potassium content.

Low magnification TEM images of the feldspar megacrysts in the 2PPG-4 sample exhibit a tweed pattern (Fig. 4a). On the [001] zone axis SAED pattern (Fig. 4a), diffuse scattering is observable along the two marked reciprocal axes, which makes a star-like shape of the diffraction spots (Fig. 4c). Such a distortion of diffraction spots indicates the simultaneous presence of albite and pericline twins (SANCHEZ-MUNOZ et al., 2012). The angle between [010]* and [100]* is 90°, which suggests monoclinic structure, however, careful observation of the diffraction spots at large scattering angles reveals that, while 90° is the dominant angle, the [010]* axis wobbles up to 0.7° in the studied volume (Fig. 4b). In some cases, clear splitting of 0*k*0 spots can also be observed. An HRTEM image shows the two orthogonal lattice distortions in more detail (Fig. 4d). Intensity variation was measured along the [010] and [100] lattice directions, and lattice periodicity was found to be constant up to 100 nm scale. Undulations of intensity maxima were found on the 10 nm scale (Figs. 4e, f) in both directions,

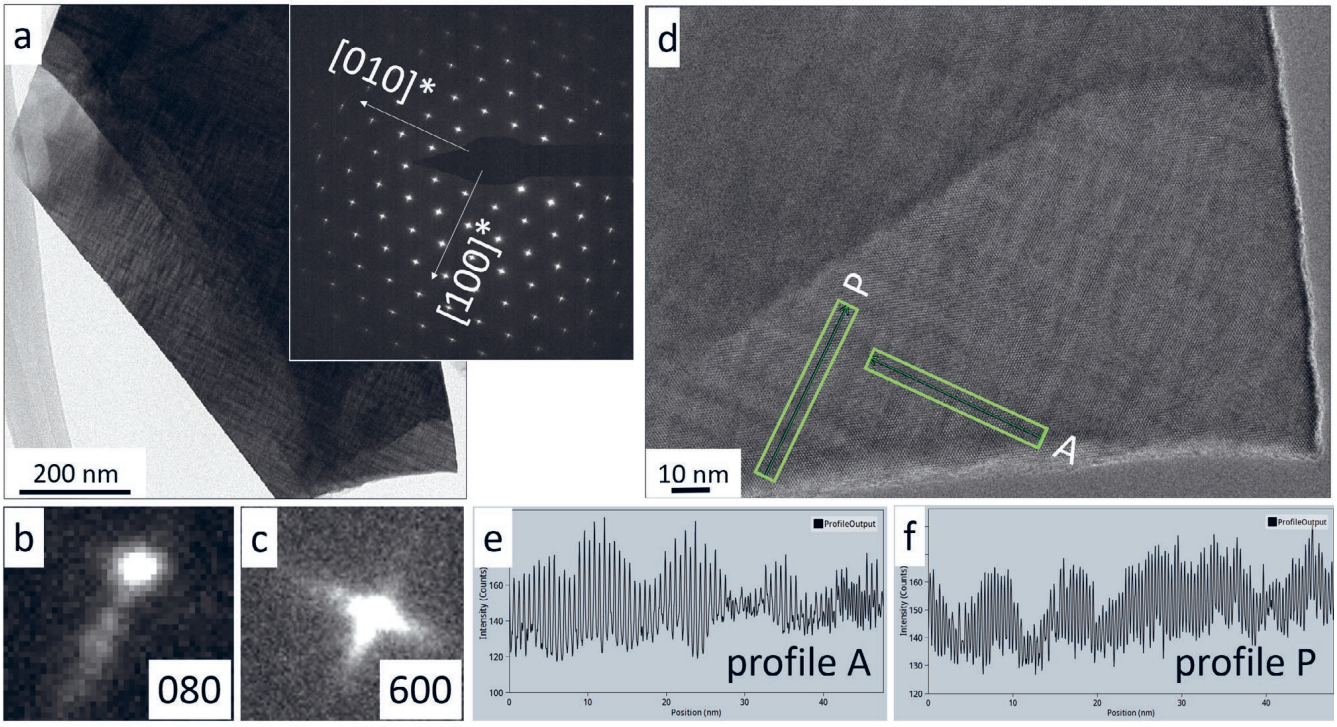

Figure 4. a) TEM bright field image of a feldspar crystal of Or(91.9)Ab(8.1)An(0) composition exhibiting tweed pattern with its [001] zone axis SAED pattern in the inset. Indexing is according to orthoclase structure; **b,c)** enlarged diffraction spots showing their typical shapes; **d)** HRTEM image of the same crystal; and **e,f)** intensity profiles along lines A and P in a 100 px wide band. Profile A and P show banding related to albite and pericline twinning.

these correspond to the thickness of albite and pericline twin lamellae. (During this analysis, a uniform sample thickness was supposed, supported by the same range of intensity variation measured in the two perpendicular directions on Fig. 4e, f).

According to TEM EDS, the feldspar from the PPG-24 sample is a plagioclase with a Na:Ca ratio close to 3:1 and minor K content (72.2%<Ab<76.5%, 23%<An<26.8%, Or<1.4%), which is in agreement with XRD results (for detailed measurement data see Suppl. 2). Besides, two low albite grains (with Ab 97 and 99%) and an anorthite grain (An=99%) were detected.

The microstructure of a plagioclase grain is presented in Figure 5. [$\bar{1}0\bar{2}$] zone axis SAED pattern is indexed according to low albite structure (Fig. 5a), however, in case of low albite, the [020]*^[20$\bar{1}$]* calculated angle is 87.5° (Fig. 5c), while the measured angle on the experimental SAED pattern is 90°, which implies monoclinic symmetry. Besides, a diffuse streaking between diffraction spots parallel to [$\bar{2}01$]* axis is observed (Fig. 5a), which implies a more complex, disordered microstructure. For a better understanding of the structural disorder, FFT analysis of HRTEM images has been performed (Fig. 5b). According to FFT analysis, the [020]*^[20$\bar{1}$]* angle exhibits certain variation as a function of location, it ranges between 86.1° and 90° (Fig. 5d). Additionally, at some locations, concentration of the diffuse scattering is observed on the FFTs halfway between the spots parallel to the [$\bar{2}01$]* axis (Fig. 5b red dotted arrows). At these locations, reflections only appear if the unit cell is larger, i.e. the c-axis is doubled with respect to albite structure. Based on these observations, we believe that the SAED represents an average structure with orthogonal (monoclinic) axes and additionally, disorder along [$\bar{2}01$]* axis. On the nano scale, at the same time, structural and/or chemical ordering has been initiated, and triclinic domains with doubled c-axis developed.

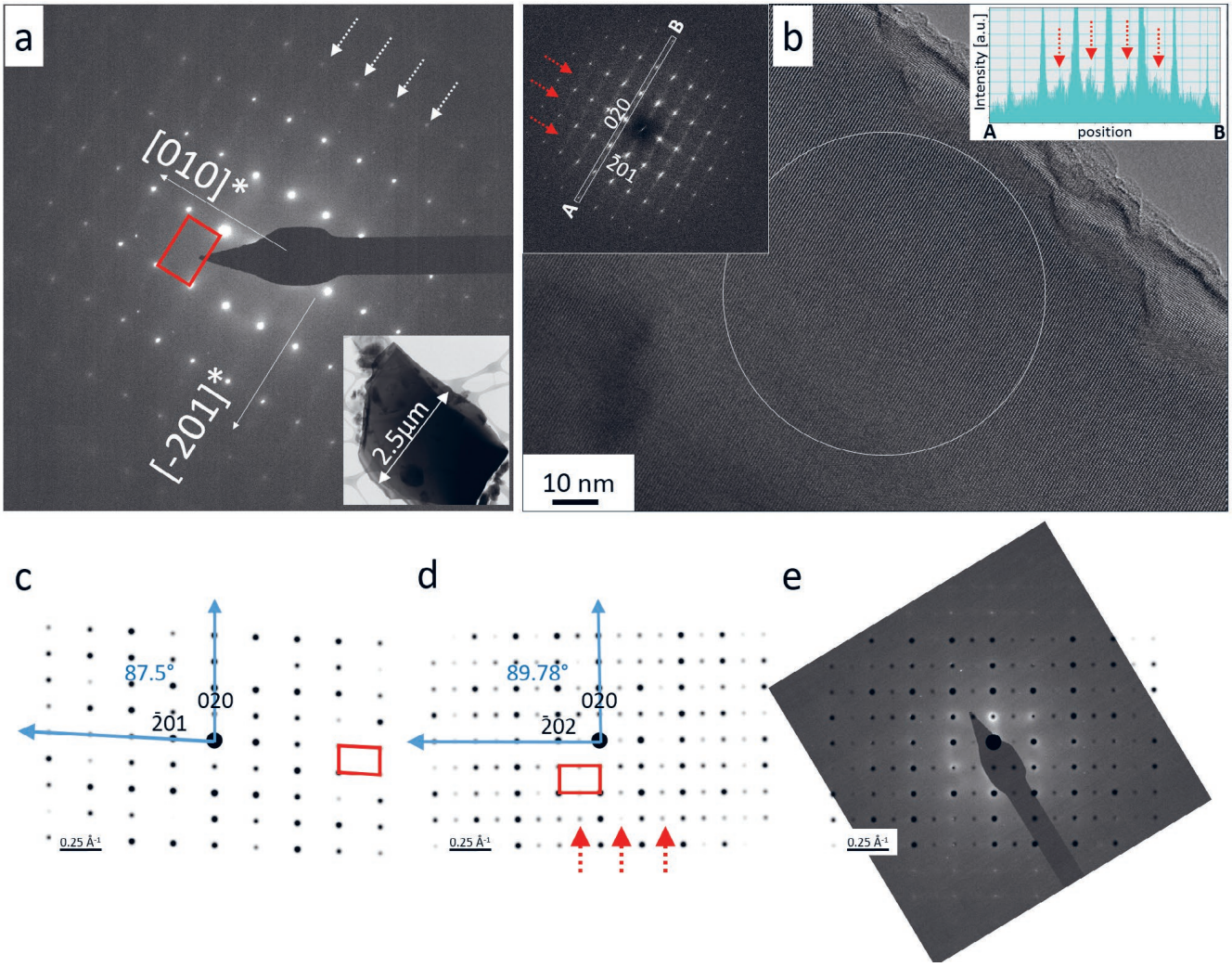

Figure 5. a) SAED pattern of a feldspar crystal of Or(1.4)Ab(72.2)An(26.4) composition (PPG-24 sample), indexed as [$\bar{1}0\bar{2}$] zone axis orientation of low albite. In the inset, the bright field image of the crystal is given. White dotted arrows indicate diffuse scattering between diffraction spots parallel to [$\bar{2}01$]* axis; **b)** HRTEM image of the same crystal. The FFT of the area indicated by a white circle is in the upper left insert. The red dotted arrows on the FFT show that half way between the spots, the diffuse scattering is concentrated. Intensity profile along the A-B band is shown in the upper right insert. Red dotted arrows indicate the half way reflections; **c)** Calculated [$\bar{1}0\bar{2}$] SAED pattern of low albite (S.G. C$\bar{1}$, a=8.142Å, b= 12.785 Å, c= 7.159 Å, α= 94.19°, α= 116.61°, α= 87.61°); and **d)** calculated SAED pattern of a high Ca containing plagioclase (S.G. I$\bar{1}$, a= 8.188 Å, b= 12. 116.04°Å, c= 14.196 Å, α= 93.37°, α= 116.04°, α= 90.87°). Red dotted arrows on (d) indicate extra spots with respect to (c); **e)** Experimental SAED pattern on (a) with the simulation shown on (d). Note a good agreement of distances and angles between simulation and SAED.

4. DISCUSSION

Although the XRPD profiles of the feldspar samples from the studied granites are quite similar, and proved to be intermediate microcline and orthoclase, (in the case of 2PPG-4) mixed with albite (2PPG-24) or albite-Ca (PPG-24), the studied feldspars show microstructural and microtextural heterogeneities under the polarized light microscope (development of twin lamellae and twin boundaries, compositional zonation), and a complex, disordered nanostructure. TEM EDS measurements of both samples are in agreement with expectations based on the XRPD results, and in the case of the PPG-24 sample, they allow the specified composition to be related to the nanostructure features.

The presence of orthoclase in the XRPD patterns of the 2PPG-4 sample indicates a minimum value for the crystallization temperature of approx. 530 C° (Fig. 6). The studied grains that showed triclinicity in their XRPD patterns, based on the splitting of (131) and ($1\bar{3}1$) reflections, reveal deviation from the monoclinic structure. Obtained values of triclinicity that reflect an ordered Al-Si distribution in the tetrahedral sites are small (Δ = 0.44, and 0.36). However, besides triclinic symmetry, the HRTEM revealed tweed nanostructure. Tweed structure forms by the simultaneous development of two independent twin systems, albite and pericline, as indicated by SAED patterns and HRTEM images (XU et al., 2000). This allows the relaxation of structural strain, which arises from the Al-Si ordering with cooling. The presence of tweed structure provides a lower limit of feldspar crystallization for deduced temperature of approximately 460 C° (GRIFFEN, 1992).

Based on TEM EDS, the PPG-24 sample contains several feldspar phases, albite anorthite and Na-Ca plagioclase (Ab:An ≈ 3:1), the latter being the most frequently measured (for detailed measurement data see Suppl. 2). This composition is in agreement with the composition of the plagioclase phase Ab=71%, An=29% (BORG & SMITH, 1968), which was identified on the XRPD pattern, besides the intermediate microcline.

Based on the HRTEM study, the plagioclase composition can be related to nanostructure characteristics, which help the understanding of crystal formation. Diffuse streaking and intensity concentration parallel to [$\bar{2}$01]* of Na-Ca plagioclase indicates a complex, disordered nanostructure and an incipient structural and/or chemical ordering in a unit cell with c≈14Å (Fig. 5e). Ordering cannot be completed because of kinetic reasons, but the triclinic structure is evident on HRTEMs (Fig. 5b).

According to the phase diagram (Fig. 7), at the Ab:An = 3:1 ratio measured in the PPG-24 sample, the plagioclase solid solution disproportionated to low albite and $I\bar{1}$ anorthite at 400 C°. The $I\bar{1}$ structure is consistent with the FFT shown on Figure 5b. The fact that no incommensurate structures have been found, suggests that the average composition of the starting material was close to the eutectic. Regarding the temperature of crystallization, we can only estimate the lowest value as 400 C°, but not the possible highest temperature at which granite crystallization started. The zonation observed under polarized light is probably related to changing composition, as supported by the different Ab:An ratios measured by TEM EDS.

The "chemically" delayed kinetics of ordering are comparable to a relatively fast cooling rate, for instance in epizonal granitoids in an anorogenic or post-tectonic environment, where the emplacement of magma in a relatively cool environment produces rocks mostly consisting of XRPD proved orthoclase (MARFUNIN, 1966; MARMO, 1971). It is in connection with the temperature decrease, when the triclinic–monoclinic transition occurs (McKENZIE, 2018).

VERNON (1986, 1990, 1999, 2004) and VERNON & PATERSON (2002) reviewed the subject of the potassium feldspar megacrysts in granite, with the conclusion that the phenocrysts evidence is favoured. The same authors suggested

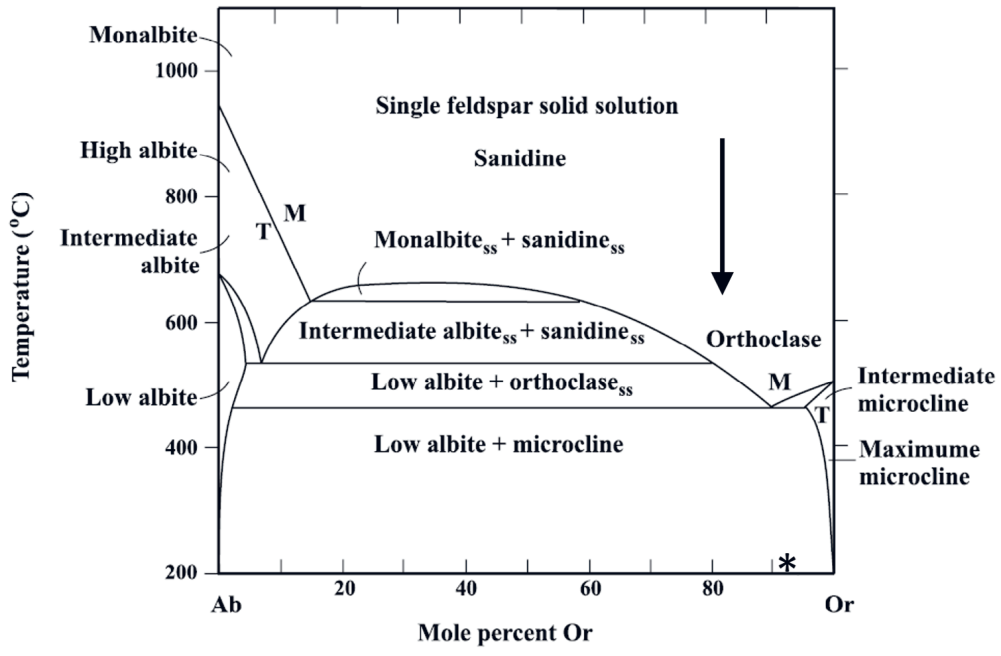

Figure 6. Estimated average composition of the starting material (arrow) and chemical composition of a feldspar megacryst (asterisks) from 2PPG-4 sample plotted on the phase diagram of alkali feldspars (after SMITH, 1974; modified by BROWN, 1981; in GRIFFEN, 1992).

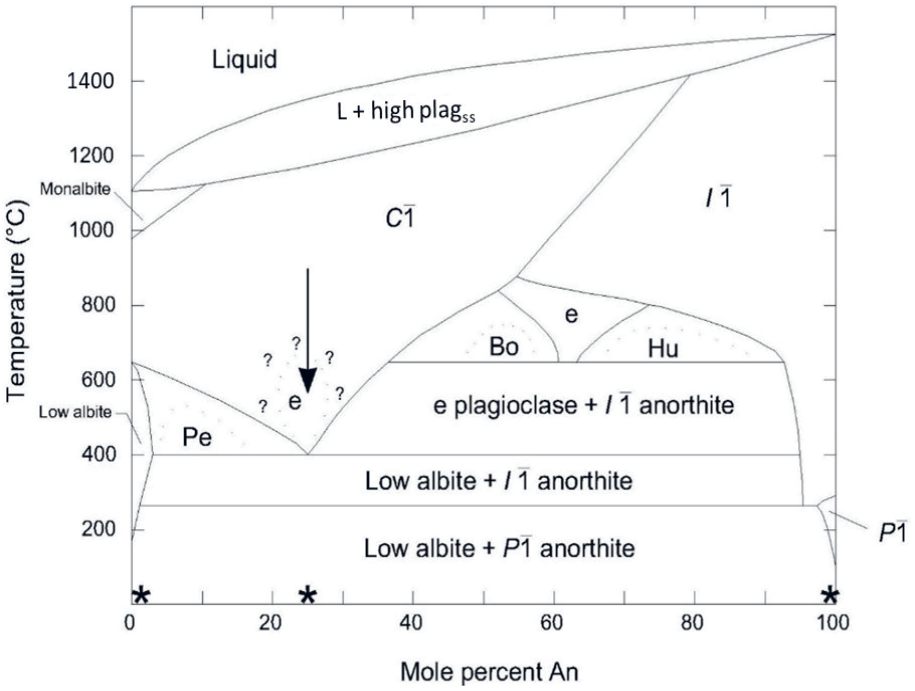

Figure 7. Estimated average composition of the starting material (arrow) and chemical composition of feldspars (asterisks) from PPG-24 sample plotted on the phase diagram for plagioclase (after CARPENTER & McCONNELL, 1984).

that K-feldspar megacrysts in granites grow late in the cooling history, even at subsolidus conditions. The experimental evidence indicates that potassium feldspar is one of the last minerals to become saturated in felsic magmas (PIWINSKII, 1968; PIWINSKII & WYLLIE, 1968; WHITNEY, 1975; CLEMENS & WALL, 1981). However, experiments also indicate that when potassium feldspar begins to crystallize, the magma typically contains 60–70% liquid (CLEMENS & WALL, 1981; WINKLER & SCHULTES, 1982). Though potassium feldspar is commonly the last mineral to begin crystallizing in granitic magmas, abundant melt is still present at that stage, allowing sufficient space for the megacrysts to grow according to VERNON (2004, and references therein). Myrmekite develops at around 450-500 ?C (TRIBE & D'LEMOS, 1996) and 500–670 °C (WIRT & VOLL, 1987), and relatively calcic plagioclase (oligoclase) in myrmekite, replaces potassium feldspar (VERNON et al., 1983) implying relatively high temperatures. The minimum temperature estimated for crystal growth is 653–439 °C for two-mica granite as given by LIU et al. (2023).

The modal composition of the two granite samples corresponds to a monzogranite–granodiorite composition according to IUGS (1973). The homogeneous structure and high plagioclase content of the sample PPG-24 most probably corresponds to higher crystallization temperatures compared to the porphyritic sample 2PPG-4, while the microstructure of the feldspars suggests parent melt close to eutectic composition for studied granites.

5. CONCLUSION

The feldspars from two different granite varieties from Pakra Creek valley (Papuk Mt.), one with a porphyritic texture and one with a homogeneous structure, were studied by optical polarizing microscopy, X-ray powder diffraction and transmission electron microscopy with energy-dispersive spectroscopy. The obtained results enable the following conclusions:

1) The porphyritic granite variety has a monzogranite composition and contains pink potassium feldspar megacrysts. Pink potassium feldspars are revealed to be orthoclase and intermediate microcline (Or > 90% and An=0). The tweed-like nanostructure provides evidence for the lower limit of potassium feldspar crystallization temperature of approximately 460 C°.

2) The homogeneous granite variety has a granodiorite composition and medium granular texture. It is abundant in plagioclase. It contains several feldspar phases: albite ($Or_{0.3}Ab_{98.7}An_1$), anorthite ($Or_0Ab_{0.5}An_{99.5}$) and Na-Ca plagioclase ($Or_{0.8}Ab_{74.1}An_{25.1}$). Under the polarizing microscope the observed potassium feldspar is orthoclase, showed as intermediate microcline in XRPD pattern, beside albite. The diffuse streaking and intensity concentration parallel to [$\bar{2}$01]* of Na-Ca plagioclase indicates structural modulations.

3) The microstructure of the feldspars suggests a parent melt close to a eutectic composition for the studied granites.

ACKNOWLEDGMENT

The presented work is the first result in the mineralogical frame of the internal research project "Complementary petrochronological characterization of granites, progressively metamorphic rocks and migmatites in the Papuk metamorphic complex (Slavonian Mts., Croatia) (PAPUKRON)" at Croatian Geological Survey, funded by National Recovery and Resilience Plan 2021–2026 of the European Union – NextGenerationEU, and monitored by the Ministry of Science, Education and Youth of the Republic of Croatia. The Authors extend their gratitude to the Department of Geology, Croatian Geological Survey's colleagues who helped in any way during the preparation of this work. The authors acknowledge the remarks and suggestions of the reviewers and associate editor, which greatly contributed to the quality of the manuscript.

REFERENCES

ALLAN, D.R. & ANGEL, R.J. (1997): A high-pressure structural study of microcline ($KAlSi_3O_8$) to 7 GPa.– European Journal of Mineralogy, 9/2, 263–275. http://doi.org/10.1127/ejm/9/2/0263

BAMBAUER, U.H., KRAUSE, C. & KROLL, H. (1989): TEM-investigation of the sanidine/microcline transition across metamorphic zones: the K-feldspar varieties.– European Journal of Mineralogy, 1, 47–58. http://doi.org/10.1127/ejm/01/1/0047

BARTH, T.F.W. (1934): Polymorphism phenomena and crystal structure.– American Journal of Science, 227, 273–286.

BATEMAN, P.C. (1992): Plutonism in the Central Part of the Sierra Nevada Batholith, California.– U.S. Geological Survey Professional Paper 1483. https://doi.org/10.3133/pp1483

BORG, I.Y. & SMITH, D.K. (1968): Calculated Powder Patterns. I. Five Plagioclases.– The American Mineralogist, 53, 1709.

BORG, I.Y. & SMITH, D.K. (1969): Calculated X-ray Powder Patterns for Silicate Minerals.– Geological Society of America, Inc. Memoir, 122, 896 p. http://doi.org/10.1130/MEM122-p1

BROWN, G. (1961): The X-ray identification and crystal structures of clay minerals.– Mineralogical Society, London, 544 p.

BROWN, G. (1981): The bond valence method: An empirical approach to chemical structure and bonding.– In: O'KEEFE, M. & NAVROTSKY, A. (eds.): Structure and bonding in crystals, Vol. 2. Academic Press, New York, 357 p. http://doi.org/10.1016/B978-0-12-525102-0.50007-4

BROWN, W.L. & PARSONS, I. (1989): Alkali feldspars: ordering rates, phase transformations and behaviour diagrams for igneous rocks.– Mineralogical Magazine, 53/369, 25–42. https://doi.org/10.1180/minmag.1989.053.369.03

CARPENTER, M.A. & McCONNELL, J.D.C. (1984): Experimental delineation of the $C\bar{1}$ and $I\bar{1}$ transormation in intermediate plagioclase feldspars.– American Mineralogists, 69, 112–121.

CLEMENS, J.D. & WALL, V.J. (1981): Origin and crystallization of some peraluminous (S-type) granitic magmas.– The Canadian Mineralogist, 9, 111–131.

COLEMAN, D.S., BARTLEY, J.M., GLAZNER, A.F. & LAW, R.D. (2005): Incremental assembly and emplacement of Mesozoic plutons in the Sierra Nevada and White and Inyo Ranges, California.– In: Geological Society of America Field Forum Field Trip Guide (Rethinking the Assembly and Evolution of Plutons: Field Tests and Perspectives, 7–14 October, 2005). https://doi.org/10.1130/2005.MCBFYT.FFG

COLLINS, L.G. & COLLINS, B.J. (2002): K-metasomatism and the origin of Ba- and inclusionzoned orthoclase megacrysts in the Papoose Flat pluton, Inyo Mountains, California, USA.– Myrmekite and Metasomatic Granite, 44, 1–70.

COX, R.A., DEMPSTER, T.J., BELL, B.R. & ROGERS, G. (1996): Crystallization of the shap granite: evidence from zoned K-feldspar megacrysts.– Journal of the Geological Society of London, 153, 625–635. http://doi.org/10.1144/gsjgs.153.4.0625

DICKSON, F.W. & SABINE, C.P. (1967): Barium-zoned large K-feldspars in quartz monzonites of eastern and southeastern California.– Geological Society of America Special Paper, 115, 323 p.

GLAZNER, A. & JOHNSON, B.R. (2013): Late crystallization of K-feldspar and the paradox of megacrystic granites.– Contributions to Mineralogy and Petrology, 166/3, https://doi.org/10.1007/s00410-013-0914-1

GLAZNER, A.F., BARTLEY, J.M., COLEMAN, D.S., GRAY, W. & TAYLOR, R.Z. (2004): Are plutons assembled over millions of years by amalgamation from small magma chambers?– GSA Today, 14/4–5. https://doi.org/10.1130/1052-5173(2004)014%3C0004:APAOMO%3E2.0.CO;2

GOLDSMITH, J.R. & LAVES, F. (1954): The microcline-sanidine stability relations.– Geochimica Cosmochimica Acta, 5, 1–19. http://doi.org/10.1016/0016-7037(54)90058-7

GRIFFEN, D.T. (1992): Silicate Crystal Chemistry.– Oxford University Press, Oxford, 442 p.

GRIM, R.E., BRAY, R.H. & BRADLEY, R.F. (1937): Mica in argillaceous sediments.– Am. Mineral., 22, 813–829.

HORVAT, M. (2004): Geochemistry and petrology of granitoids of Papuk and Psunj Mts. (Slavonia, Croatia).– Unpubl. PhD Thesis, University of Budapest, Budapest, Hungary (133+108) p.

HORVAT, M., TIBLJAŠ, D., BUDA, GY. & LOVAS, GY. (2011): X-ray study of potassium feldspars from different granitoid types and gneisses of Papuk Mt. (Slavonia, Croatia).– Geologia Croatica, 64/2, 153–162. https://doi.org/104154/gc.2011.13

HOVMÖLLER, S (1992): CRISP: crystallographic image processing on a personal computer.– Ultramicroscopy, 41, 121–135. https://doi.org/10.1016/0304-3991(92)90102-P

IUGS Subcommission on the Systematics of Igneous Rocks (1973): Classification and Nomenclature of Plutonic Rocks. Recommendations.– Neues Jahrbuch fur Mineralogie Abhandlungen, H 4, 149–164.

JAMIČIĆ, D. (2001): Main geological features of the Slavonian Mts. focused to the Našice area.– Matica Hrvatska, Našički zbornik, 6, 29–36.

JOHNSON, B.R., GLAZNER, A.F. & COLEMAN, D.S. (2006a): Significance of K-feldspar megacryst size and distribution the Tuolumne Intrusive Suite, California.– Geological Society of America, Abstracts with Programs, 38, 93.

JOHNSON, B.R., GLAZNER, A.F. & COLEMAN, D.S. (2006b): Potassium feldspar megacrysts in granites: passive markers of magma dynamics or products of textural coarsening?– EOS Transactions of the American Geophysical Union, 87/52, V51B–1670.

KERRICK, D.M. (1969): K-feldspar megacrysts from a porphyritic quartz monzonite, central Sierra Nevada, California.– The American Mineralogist, 54, 839–848.

KONTONIKAS-CHAROS, A., CIOBANU, C.L., COOK, N.J., EHRIG, K., RISMAIL†, R., KRNETA, S. & BASAK, A. (2018): Feldspar mineralogy and rare-earth element (re)mobilization in iron-oxide copper gold systems from South Australia: a nanoscale study.– Mineralogical Magazine, 82/S1, S173–S197. http://doi.org/10.1180/minmag.2017.081.040

KOVÁCS KIS, V., HORVAT, M. & DÓDONY, I. (2004): Microstructures in two alkali feldspar megacrysts from the Papuk Mt., Croatia.– Geologia Croatica, 57/2, 149–158. https://doi.org/10.4154/GC.2004.12

KUČAN, F. & KRMPOTIĆ, M. (1911): Microclinemicroperthite from Pakra [in Croatian].– Glasnik hrvatskog prirodoslovnog društva. Godište XXIII, Zagreb, 104–107.

LAVES, F. (1950): The lattice and twinning of microcline and other potash feldspar.– Journal of Geology, 58, 548–571.

LAVES, F. & GOLDSMITH, J.R. (1961): Polymorphism, order, disorder, diffusion and confusion in the feldspars.– Estudos Geologicos, Cursillos y Conferencias, 8, 71–80.

LIU, Y., QIN, K., ZHAO, J., ZHOU, Q., SHI, R., HE, C. & GAO, Y. (2023): Feldspar traces mineralization processes in the Qongjiagang giant lithi-

um ore district, Himalaya, Tibet.– Ore Geology Reviews, 157/105451. https://doi.org/10.1016/j.oregeorev.2023.10545

MARFUNIN, A.S. (1966): The Feldspars. Phase Relations, Optical Properties, and Geological Distribution.– Israel Program for Scientific Translations, Jerusalem, Israel.

MARMO, V. (1971): Granite Petrology and the Granite Problem.– Elsevier, New York.

McKENZIE, W.S. (2018): The orthoclase-microcline inversion.– Mineralogical Magazine and Journal of the Mineralogical Society, 30/225, 354–366. https://doi.org/10.1180/minmag.1954.030.225.03

McLAREN, A.C. (1984): Transmission electron microscope investigations of the microstructures of microclines.– In: BROWN, W.L. (ed.): Feldspars and feldspathoids. NATO ASI series, ser C. 137, 373–409. http://doi.org/10.1007/978-94-015-6929-3_10

MORRIS, M.C., McMURDIE, H.F., EVANS, E.H., PARETZKIN, B., PARKER, H.S. & PANAGIOTOPOULOS, N.C. (1981): Standard X-ray Diffraction Powder Patterns Section 18 – Data for 58 Substances. Silicon oxide (quartz, low), a-SiO_2.– National Bureau of Standards Monograph, 25, 61 p.

NAVROTSKY, A. (2011): Nanoscale effects on thermodynamics and phase equilibria in oxide systems.– ChemPhysChem, 12, 2207–2215. http://doi.org/10.1002/cphc.201100129

NAVROTSKY, A., MAZEINA, L. & MAJZLAN, J. (2008): Size-driven structural and thermodynamic complexity in iron oxides.– Science, 319, 1635–1638. http://doi.org/10.1126/science.1148614

PAKHOMOV, V.I., GORYUNOV, A.V., PAKHOMOV, P.V. & CHIBISKOVA, N.T. (1993): On the structure of alpha-SiO_2 crystals doped with Fe^{3+}.– Zhurnal Neorganicheskoi Khimii, 38, 39–44.

PANalytical (2016): X'Pert Software HighScore Plus, Version 4.5 (4.5.0.22741), Almeo, The Netherlands.

PARSONS, I., GERALD, J.D.F. & LEE, M.R. (2015): Routine characterization and interpretation of complex alkali feldspar intergrowths.– American Mineralogist, 100/5–6, 1277–1303. http://doi.org/10.2138/am-2015-5094

PIWINSKII, A.J. (1968): Experimental studies of igneous rock series, central Sierra Nevada Batholith, California.– Journal of Geology, 76, 548–570. http://doi.org/10.1086/627359

PIWINSKII, A.J. & WYLLIE, P.J. (1968): Experimental studies of igneous rock series: a zoned pluton in the Wallowa Batholith, Oregon.– Journal of Geology, 76, 205–234. http://doi.org/10.1086/627323

POLJAK, J. (1952): Predpaleozojske i paleozojske naslage Papuka i Krndije [*Paleozoic and before Paleozoic deposits of Papuk and Krndija* – in Croatian].– Geološki vjesnik, 2-4, 63–82.

PRINCE, E., DONNAY, G. & MARTH, R.F. (1973): Neutron diffraction refinement of an ordered orthoclase structure.– American Mineralogist, 58/5–6, 500–507.

RIBBE, P.H. (ed.) (1983): Feldspar Mineralogy.– Reviews in Mineralogy, Mineralogical Society of America, Chantilly, Virginia.

ROCKHOLD, J.R., NABELEK, P.I. & GLASCOCK, M.D. (1987): Origin of rhythmic layering in the Calamity Peak satellite pluton of the Harney Peak Granite, South Dakota: the role of boron.– Geochim Cosmochim Acta, 51, 487–496. http://doi.org/10.1016/0016-7037(87)90063-9

SÁNCHEZ-MUÑOZ, L., GARCÍA-GUINEA, J., ZAGORSKY, V.YE., JUWONO, T., MODRESKI, P.J., CREMADES, A., VAN TENDELOO, G. & DE MOURA, O.J.M. (2012): The evolution of twin patterns in perthitic K-feldspar from granitic pegmatites.– The Canadian Mineralogist, 50, 989–1024. https://doi.org/10.3749/canmin.50.4.989

SCHMID, S.M., FÜGENSCHUH, B., KOUNOV, A., MATENCO, L., NIEVERGELT, P., OBERHÄNSLI, R., PLEUGER, J., SCHEFER, S., SCHUSTER, R., TOMLJENOVIĆ, B., USTASZEWSKI, K. & VAN HINSBERGEN, D.J.J. (2020): Tectonic units of the Alpine collision zone between Eastern Alps and western Turkey.– Gondwana Research, 78, 308–374. https://doi.org/10.1016/j.gr.2019.07.005

SMITH, J.V. (1956): Geology and Mineralogy. Structural Control of Polymorphism in Micas.– Nature, 4656, p. 253.

SMITH, J.V. (1974): Feldspar Minerals. I. Crystal structure and physical properties.– Springer-Verlag, Heidelberg, 627 p.

STEWART, D.B. & RIBBE, P.H. (1983): Optical properties of feldspars.– In: RIBBE, P.H. (ed.): Feldspar Mineralogy, Reviews in Mineralogy and Geochemistry, 2, 121–139. https://doi.org/10.1515/9781501508547-010

TAJDER, M. (1957): Petrographic investigation of the western part of the Papuk Mt [in Croatian].– Ljetopis JAZU, 62, 316–323.

TRIBE, I.R. & D'LEMOS, R.S. (1996): Significance of a hiatus in down-temperature fabric development within syn-tectonic quartz diorite complexes, Channel Islands, UK.– Journal of the Geological Society of London, 153, 127–138. http://doi.org/10.1144/gsjgs.153.1.0127

VERNON, R.H. (1986): K-feldspar megacrysts in granites – Phenocrysts, not porphyroblasts.– Earth-Science Reviews, 23/1, 1–63. https://doi.org/10.1016/0012-8252(86)90003-6

VERNON, R.H. (1990): K-feldspar augen in felsic gneisses and mylonites– deformed phenocrysts or porphyroblasts?– Geologiska Föreningens i Stockholm Förhandlingar, 112, 157–167. http://doi.org/10.1080/11035899009453175

VERNON, R.H. (1999): Quartz and feldspar microstructures in metamorphic rocks.– Canadian Mineralogist, 37, 513–524.

VERNON, R.H. (2004): A Practical Guide to Rock Microstructure.– Cambridge University Press, Cambridge, 594 p. http://doi.org/10.1017/CBO9780511807206

VERNON, R.H. & PATERSON, S.R. (2002): Igneous origin of K-feldspar megacrysts in deformed granites of the Papoose Flat pluton, California, USA.– Electronic Geosciences, 7, 31–39. http://doi.org/10.1007/s10069-002-0005-3

VERNON, R.H., WILLIAMS, V.A. & D'ARCY, W.F. (1983): Grainsize reduction and foliation development in deformed granitoid batholith.– Tectonophysics, 92, 123–145.

VRAGOVIĆ, M. (1965): Granites and gneisses of the Papuk Mountain [in Croatian].– Unpubl. PhD Thesis. Sveučilište u Zagrebu, Prirodoslovno-matematički fakultet, Zagreb, 1-XY p.

WARR, L.N. (2021): IMA-CNMNC approved mineral symbols.– Mineralogical Magazine, 85, 291–320. https://doi.org:10.1180/mgm.2021.43

WEBBER, K.L., SIMMONS, W.B., FALSTER, A.U. & FOORD, E.E. (1999): Cooling rates and crystallization dynamics of shallow level pegmatite-aplite dikes, San Diego County, California.– American Mineralogist, 84, 708–717. http://dx.doi.org/10.2138/am-1999-5-602

WHITNEY, J.A. (1975): The effects of pressure, temperature, and XH2O on phase assemblages in four synthetic rock compositions.– Journal of Geology, 83, 1–31.

WILLAIME, C., BROWN, W.L. & GANDAIS, G. (1976): Physical aspects of exolution in natural alkali feldspars.– In: WENK, H.R. (ed.): Electron Microscopy in Mineralogy. Springer-Verlag, Berlin, 248–257.

WINKLER, H.G.F. & SCHULTES, H. (1982): On the problem of alkali feldspar phenocrysts in granitic rocks.– Neues Jahrbuch für Mineralogie Monatshefte, 12, 558–564.

WIRT, R. & VOLL, G. (1987): Cellular intergrowth between quartz and sodium-rich plagioclase (myrmekite) – an analogue of discontinuous precipitation in metal alloys.– Journal of Materials Science, 22, 1913–1918. http://dx.doi.org/10.1007/BF01132916

XU, H., VEBLEN, D.R., BUSECK, P. & RAMAKRISHNA, B.L. (2000): TEM and SFM of exsolution and twinning in an alkali feldspar.– American Mineralogist, 85, 509–514. http://doi.org/10.2138/am-2000-0412

Supplement 1. – TEM EDS measurements of grains from sample 2PPG-4.

2PPG-4 sample, pink grain 2024/08/01 analysis number 0928 – Or(1.2)Ab(98.8)An(0)

Z	Element	Family	Atomic Fraction (%)	Atomic Error (%)	Mass Fraction (%)	Mass Error (%)	Fit Error (%)
8	O	K	61.45	3.06	48.65	3.31	0.38
11	Na	K	7.34	1.41	8.35	1.63	1.66
13	Al	K	7.63	1.44	10.19	1.93	0.96
14	Si	K	23.49	3.49	32.65	4.31	0.68
19	K	K	0.09	0.02	0.17	0.03	2.54

2PPG-4 sample, pink grain 2024/08/01 analysis number 1030 – Or(91.8)Ab(8.2)An(0)

Z	Element	Family	Atomic Fraction (%)	Atomic Error (%)	Mass Fraction (%)	Mass Error (%)	Fit error (%)
8	O	K	60.69	6.70	45.40	3.21	2.11
11	Na	K	0.63	0.14	0.67	0.14	1.03
13	Al	K	8.34	1.88	10.52	2.20	1.76
14	Si	K	23.41	5.18	30.74	6.29	1.58
19	K	K	6.93	1.43	12.67	2.39	0.40
20	Ca	K	0.00	0.00	0.00	0.00	0.00

2PPG-4 sample, pink grain 2024/08/01 analysis number 1045 – Or(89.5)Ab(10.5)An(0)

Z	Element	Family	Atomic Fraction (%)	Atomic Error (%)	Mass Fraction (%)	Mass Error (%)	Fit error (%)
8	O	K	60.78	6.90	45.83	3.32	2.03
11	Na	K	0.65	0.15	0.70	0.15	1.11
13	Al	K	8.30	1.89	10.56	2.22	1.51
14	Si	K	24.77	5.52	32.78	6.72	1.33
19	K	K	5.50	1.15	10.13	1.92	0.34
20	Ca	K	0.00	0.00	0.00	0.00	0.00

2PPG-4 sample, pink grain 2024/08/01 analysis number 1047 – Or(93.3)Ab(6.7)An(0)

Z	Element	Family	Atomic Fraction (%)	Atomic Error (%)	Mass Fraction (%)	Mass Error (%)	Fit Error (%)
8	O	K	61.66	2.98	46.31	3.03	0.38
11	Na	K	0.51	0.11	0.55	0.12	5.92
13	Al	K	7.90	1.49	10.01	1.90	2.29
14	Si	K	22.87	3.42	30.16	4.15	1.04
19	K	K	7.07	1.20	12.97	2.14	0.16
20	Ca	K	0.00	0.00	0.00	0.00	515.82

2PPG-4 sample, pink grain 2024/08/01 analysis number 1136 – Or(86.6)Ab(13.4)An(0)

Z	Element	Family	Atomic Fraction (%)	Atomic Error (%)	Mass Fraction (%)	Mass Error (%)	Fit Error (%)
8	O	K	61.00	3.02	45.84	3.05	0.74
11	Na	K	1.00	0.20	1.08	0.23	1.14
13	Al	K	7.95	1.49	10.07	1.90	1.27
14	Si	K	23.54	3.50	31.05	4.22	1.35
19	K	K	6.51	1.12	11.95	2.00	0.07
20	Ca	K	0.00	0.00	0.01	0.00	19.49

2PPG-4 sample, pink grain 2024/09/24 analysis number 1259 – Or(91.9)Ab(8.1)An(0)

Z	Element	Family	Atomic Fraction (%)	Atomic Error (%)	Mass Fraction (%)	Mass Error (%)	Fit error (%)
8	O	K	61.42	6.56	46.18	3.13	1.58
11	Na	K	0.59	0.13	0.64	0.13	2.18
13	Al	K	8.43	1.89	10.69	2.23	0.93
14	Si	K	22.83	5.02	30.13	6.14	1.11
19	K	K	6.73	1.38	12.36	2.32	0.41
20	Ca	K	0.00	0.00	0.00	0.01	0.00

2PPG-4 sample, pink grain 2024/09/24 analysis number 1231 – Or(94.8)Ab(5.2)An(0)

Z	Element	Family	Atomic Fraction (%)	Atomic Error (%)	Mass Fraction (%)	Mass Error (%)	Fit error (%)
8	O	K	60.09	6.72	44.97	3.14	0.42
11	Na	K	0.33	0.08	0.36	0.07	1.33
13	Al	K	8.41	1.91	10.61	2.22	0.96
14	Si	K	25.09	5.59	32.96	6.76	1.20
19	K	K	6.07	1.27	11.11	2.10	0.58
20	Ca	K	0.00	0.00	0.00	0.00	0.00

2PPG-4 sample, pink grain 2024/09/24 analysis number 1135 – Or(91.1)Ab(8.9)An(0)

Z	Element	Family	Atomic Fraction (%)	Atomic Error (%)	Mass Fraction (%)	Mass Error (%)	Fit Error (%)
8	O	K	61.64	2.99	46.47	3.04	0.85
11	Na	K	0.62	0.13	0.68	0.14	0.75
13	Al	K	8.41	1.57	10.69	2.00	1.15
14	Si	K	22.88	3.42	30.28	4.16	0.74
19	K	K	6.45	1.10	11.88	1.98	0.35
20	Ca	K	0.00	0.00	0.00	0.00	0.00

Supplement 2. – TEM EDS measurements of grains from sample PPG-24.

PPG-24 sample, white grain 2024/08/01 analysis number 1316 – Or(0.5)Ab(76.5)An(23)

Z	Element	Family	Atomic Fraction (%)	Atomic Error (%)	Mass Fraction (%)	Mass Error (%)	Fit Error (%)
8	O	K	61.08	2.80	47.67	2.94	0.59
11	Na	K	6.63	1.28	7.44	1.45	1.88
13	Al	K	9.85	1.80	12.96	2.35	1.43
14	Si	K	20.40	3.16	27.94	3.96	0.95
19	K	K	0.05	0.01	0.09	0.02	5.31
20	Ca	K	1.99	0.28	3.90	0.55	0.28

PPG-24 sample, white grain 2024/08/01 analysis number 1322 – Or(0)Ab(0.7)An(99.3)

Z	Element	Family	Atomic Fraction (%)	Atomic Error (%)	Mass Fraction (%)	Mass Error (%)	Fit Error (%)
8	O	K	56.85	2.68	40.80	2.49	0.63
11	Na	K	0.08	0.02	0.08	0.02	7.85
13	Al	K	16.88	2.83	20.44	3.35	1.26
14	Si	K	15.61	2.59	19.67	3.18	0.33
19	K	K	0.00	0.00	0.00	0.00	0.00
20	Ca	K	10.57	1.34	19.01	2.30	0.22

PPG-24 sample, white grain 2024/08/01 analysis number 1412 – Or(1.4)Ab(72.2)An(26.4)

Z	Element	Family	Atomic Fraction (%)	Atomic Error (%)	Mass Fraction (%)	Mass Error (%)	Fit Error (%)
8	O	K	57.37	3.00	43.71	3.01	1.27
11	Na	K	5.66	1.11	6.20	1.24	1.11
13	Al	K	10.98	2.00	14.11	2.55	0.67
14	Si	K	23.80	3.54	31.82	4.29	0.45
19	K	K	0.11	0.02	0.21	0.04	1.37
20	Ca	K	2.07	0.29	3.95	0.57	0.39

PPG-24 sample, white grain 2024/09/24 analysis number 1355 – Or(0.6)Ab(99.4)An(0)

Z	Element	Family	Atomic Fraction (%)	Atomic Error (%)	Mass Fraction (%)	Mass Error (%)	Fit Error (%)
8	O	K	62.80	2.97	50.10	3.26	0.60
11	Na	K	7.28	1.39	8.34	1.62	0.90
13	Al	K	7.71	1.45	10.37	1.95	1.22
14	Si	K	22.06	3.33	30.90	4.18	0.24
19	K	K	0.04	0.01	0.08	0.01	2.73

PPG-24 sample, white grain 2024/09/24 analysis number 1409 – Or(0.3)Ab(97.5)An(2.3)

Z	Element	Family	Atomic Fraction (%)	Atomic Error (%)	Mass Fraction (%)	Mass Error (%)	Fit error (%)
8	O	K	61.46	6.62	48.60	3.28	0.09
11	Na	K	7.01	1.58	7.96	1.67	0.59
13	Al	K	8.08	1.82	10.77	2.25	0.07
14	Si	K	23.27	5.13	32.30	6.59	0.06
19	K	K	0.02	0.00	0.03	0.01	7.48
20	Ca	K	0.17	0.03	0.33	0.05	0.90

PPG-24 sample, white grain 2024/09/24 analysis number 1427 – Or(0)Ab(0.3)An(99.7)

Z	Element	Family	Atomic Fraction (%)	Atomic Error (%)	Mass Fraction (%)	Mass Error (%)	Fit Error (%)
8	O	K	57.79	2.77	41.82	2.62	2.91
11	Na	K	0.03	0.01	0.03	0.01	10.30
13	Al	K	16.18	2.75	19.75	3.28	1.51
14	Si	K	16.08	2.66	20.42	3.27	0.26
19	K	K	0.00	0.00	0.00	0.00	0.00
20	Ca	K	9.92	1.28	17.99	2.21	0.09

PPG-24 sample, white grain 2024/10/09 analysis number 1030 – Or(0.2)Ab(76.5)An(23.3)

Z	Element	Family	Atomic Fraction (%)	Atomic Error (%)	Mass Fraction (%)	Mass Error (%)	Fit error (%)
8	O	K	62.41	6.36	49.34	3.20	1.53
11	Na	K	6.47	1.44	7.35	1.53	0.22
13	Al	K	9.19	2.04	12.25	2.54	0.35
14	Si	K	20.87	4.53	28.96	5.87	0.14
19	K	K	0.01	0.00	0.03	0.01	7.70
20	Ca	K	1.05	0.18	2.08	0.31	0.11

PPG-24 sample, white grain 2024/10/09 analysis number 1103 – Or(0.8)Ab(72.4)An(26.8)

Z	Element	Family	Atomic Fraction (%)	Atomic Error (%)	Mass Fraction (%)	Mass Error (%)	Fit error (%)
8	O	K	61.27	6.16	47.73	3.02	0.86
11	Na	K	5.41	1.21	6.06	1.26	2.06
13	Al	K	10.44	2.31	13.72	2.84	0.68
14	Si	K	20.81	4.52	28.46	5.76	0.17
19	K	K	0.07	0.01	0.12	0.02	2.57
20	Ca	K	2.00	0.33	3.91	0.57	0.32

PPG-24 sample, white grain 2024/10/09 analysis number 1140 – Or(0.9)Ab(73)An(26.1)

Z	Element	Family	Atomic Fraction (%)	Atomic Error (%)	Mass Fraction (%)	Mass Error (%)	Fit Error (%)
8	O	K	59.78	3.08	46.18	3.19	2.60
11	Na	K	4.42	0.88	4.91	0.99	0.27
13	Al	K	11.00	2.01	14.33	2.59	1.32
14	Si	K	23.15	3.48	31.40	4.27	0.95
19	K	K	0.06	0.01	0.11	0.02	4.95
20	Ca	K	1.58	0.22	3.06	0.45	0.17